RSC Advances

ROYAL SOCIETY OF CHEMISTRY

www.rsc.org/advances

Polystyrene Grafted Graphene Nanoplatelets with Various Graft Densities by Atom Transfer Radical Polymerization from the Edge Carboxyl Groups

Hossein Roghani-Mamaqani[1]*, Vahid Haddadi-Asl[2], Khezrollah Khezri[3], Mehdi Salami-Kalajahi[1]

[1] Department of Polymer Engineering, Sahand University of Technology, P.O. Box 51335-1996, Tabriz, Iran.

[2] Department of Polymer Engineering and Color Technology, Amirkabir University of Technology, P.O. Box 15875-4413, Tehran, Iran.

[3] School of Chemistry, University College of Science, University of Tehran, P.O. Box 14155-6455, Tehran, Iran.

Graphical Abstract

An initiator and hydroxyl containing modifier, 4-hydroxybutyl 2-bromopropionate (CBr), was synthesized by coupling reaction of 1,4-butanediol and alpha-bromoisobutyryl bromide. Subsequently, graphene oxide (GO) was functionalized with CBr from the edge carboxyl groups to yield initiator-anchored graphene (GCBr). Then, GCBr was used as the precursor for ATRP of styrene to evaluate the effect of graphene loading and graft density on the products properties.

* Corresponding author. Tel/Fax: +98 411 3459089. E-mail address: r.mamaghani@sut.ac.ir
(H. Roghani-Mamaqani)

Styrene, PMDETA, EBrP

110 °C

GCBr

Attached Polystyrene Chains

PLA

PHA

Free Polystyrene Chains

Attached Polystyrene Chains

Graphene/Polystyrene nanocomposite

Polystyrene Grafted Graphene Nanoplatelets with Various Graft Densities by Atom Transfer Radical Polymerization from the Edge Carboxyl Groups

Hossein Roghani-Mamaqani[1]*, Vahid Haddadi-Asl[2], Khezrollah Khezri[3], Mehdi Salami-Kalajahi[1]

[1] Department of Polymer Engineering, Sahand University of Technology, P.O. Box 51335-1996, Tabriz, Iran.

[2] Department of Polymer Engineering and Color Technology, Amirkabir University of Technology, P.O. Box 15875-4413, Tehran, Iran.

[3] School of Chemistry, University College of Science, University of Tehran, P.O. Box 14155-6455, Tehran, Iran.

ABSTRACT

An initiator and hydroxyl containing modifier, 4-hydroxybutyl 2-bromopropionate (CBr), was synthesized through the coupling reaction of 1,4-butanediol and alpha-bromoisobutyryl bromide.

* Corresponding author: Tel/Fax: +98 411 3459089. E-mail address: r.mamaghani@sut.ac.ir (H. Roghani-Mamaqani)

1

Subsequently, graphene oxide (GO) was functionalized with CBr from the edge carboxyl groups by an esterification reaction to yield initiator-anchored graphene nanoplatelets (GCBr). Then, GCBr was used in different amounts as the precursor for atom transfer radical polymerization of styrene for evaluation of the effect of graphene loading and graft density on the kinetics and properties of the products. Successful edge-functionalization of GO with CBr and polystyrene was also proved by FTIR. Carbon and Bromine ratio of 21.92 from the results of XPS shows that about 1 molecule of CBr was attached to every 3.65 aromatic ring of GCBrH. GPC results show that molecular weight and PDI values of the attached chains are higher, and molecular weight and conversion values increase by increasing grafting density. The amount of modifier and polystyrene attachment to the graphene edge was evaluated by TGA. Relaxation behavior of chains in the presence of graphene layers and also effect of graft content on the chain confinement were studied using DSC. The ordered and disordered crystal structure of carbon was evaluated by Raman spectroscopy. The same XRD angle for the high and low graft densities at 7.5° shows that expansion of graphene interlayer is independent from the population of attached chains to the graphene edge. Finally, opaque and wrinkled morphology of graphene nanoplatelets was observed by scanning and transmission electron microscopy.

INTRODUCTION

Polymer grafting is an interesting subject in the field of polymer nanocomposites and especially surface modification processes. Three methods of "grafting from", "grafting through", and "grafting to" have commonly been used for covalent grafting of polymers [1]. In "grafting from" technique, polymer chains propagate from the surface-attached initiators [2–6]. The "grafting through" method is based on the incorporation of surface-attached double bonds into polymer chains during propagation reaction [7–12]. In "grafting to" technique, end group transformed polymer chains react with the functional groups of substrates and forms graft polymer chains [13]. Grafting preformed polymer chains directly to a substrate is not ideal because of steric restrictions. However, grafting polymer units from the initiator moieties attached to a substrate results in a high degree of control over grafting density and thickness of the polymer brushes [2]. Functional groups play a key role in the grafting reactions. Initiator attachment on the surfaces, anchoring double bond containing moieties, and also coupling reactions like click chemistry, esterification, amidation, and radical coupling make the functional groups based polymerization methods very important in graft polymerization [14–17].

Graphene nanoplatelets with its extraordinary physical properties considered as high-performance nanomaterials [18, 19]. Graphene is composed of sp^2-hybridized carbon atoms arranged in a honeycomb structure. A strong π-π interaction between the nanoplatelets restricts its dispersability in various solvents and polymers. Therefore, functionalization of graphene nanoplatelets, physically or chemically, is a crucial factor in the synthesis of graphene nanocomposites. Similar to carbon nanotubes, functionalization of graphene nanoplatelets with covalent or non-covalent bonding enhances its dispersibility in various media [20, 21]. Chemical oxidation and exfoliation of graphite is one of the most important routs to prepare graphene

oxide (GO). GO has lots of oxygen containing functional groups, such as hydroxyl and epoxide in the basal plane and carboxyl at the edges [19]. High value of these functional groups makes it possible to functionalize GO by carboxylic acid based esterification or epoxy based ring opening reactions [18]. Also, functional groups make GO to be easily dispersed in polar solvents which facilitate production of polymer nanocomposites by solution blending. However, reduction of the nanoplatelets may cause irreversible stacking because of the strong π-π interactions. Polymer functionalization weakens these interactions by providing a distance between the layers. Therefore, covalent attachment of polymer chains from the edge or surface functional groups can be an effective rout to reduce the stacking of these nanoplatelets after reduction.

Functional polymers have commonly been synthesized by controlled radical polymerization (CRP), which is based on reversible termination or transfer reactions by radicals and functional groups [22]. Among various CRP approaches, atom transfer radical polymerization (ATRP) which is based on reversible termination of growing radicals by a halogen atom has been considered largely. Integrating ATRP with various grafting reaction makes it possible to selectively functionalize various substrates and benefits from the post polymerization modifications. Polymer functionalization of graphene nanoplatelets has been carried out frequently from the surface and edge functional groups by using various grafting reactions [2–6, 23–32]. Among the various grafting techniques, "grafting from" has been employed frequently with ATRP. Considering the hydroxyl groups, Lee et al. synthesized covalently attached polystyrene chains from the surface of graphene nanoplatelets [2]. Fang et al. covalently attached polystyrene chains on the graphene surface via a different procedure of diazonium and ATRP initiator introduction to the reduced GO surface [5]. They also carried out an interesting research on the controlled grafting of polystyrene chins from the surface of initiator-functionalized

4

graphene nanoplatelets [6]. They controlled grafting density and polystyrene chain lengths by modulating the concentrations of diazonium compound during the grafting of initiator and also monomer in ATRP. Zhu et al. directly attached alpha-bromoisobutyryl bromide (BiBB) to the surface of GO and subsequently synthesized thermoresponsive PNIPAAm chains by ATRP [23]. Surface hydroxyl groups were also used in other grafting reactions. In situ thermal polymerization was accomplished by Bao et al. to obtain epoxy resin-attached graphene nanocomposites [24]. They functionalized graphene oxide by hexachlorocyclotriphosphazene and glycidol and then incorporated it into epoxy resin. Bao et al. functionalized graphene oxide with char-catalyzing agents and reactive compounds of hexachlorocyclotriphosphazene and incorporated it into polystyrene by a grafting through reaction [25]. Lin et al. coated Gamma-aminopropyltriethoxysilane (APTES) onto the graphene oxide sheets, and then grafted maleic anhydride grafted polyethylene onto the APTES coated graphene oxide sheets by a "grafting onto" reaction [26]. Graphene oxide surface epoxide groups was also used to cover the graphene surface with polymer chains. Deng et al. reported the attachment of PNIPAAm chains with controlled grafting via *in situ* single-electron transfer living radical polymerization (SET–LRP) [3]. Exfoliated GO sheets were sequentially subject to an epoxide ring opening reaction with tris(hydroxymethyl) aminomethane (TRIS) to increase the amount of reactive sites, esterification with BiBB to introduce the initiator groups on both hydroxyl and epoxide functional groups, and finally surface-initiated single electron transfer living radical polymerization of NIPAAm. They also attached poly(ethylene glycol) ethyl ether methacrylate chains from the surface of GO similar to this procedure [27]. Edge carboxyl functional groups of GO were also used as the precursor to polymer functionalize graphene nanoplatelets. Concalves et al. used BiBB-functionalized graphene nanoplatelets for grafting PMMA from the edges [4]. Also Ren et al.

used the similar procedure for grafting polystyrene and PMMA [28]. Yang et al. converted the carboxyl groups of GO to amine functionality by reacting with 1,3-Diaminopropane and prepared GO nanoplatelets with hydroxyl and amine groups. Then, poly(2-(dimethylamino)ethyl methacrylate) was grown from the BiBB-attached hydroxyl and amine groups [29]. Zhang et al. synthesized PA6-grafted GO by in situ grafting from anionic ring-opening polymerization. They attached ε-caprolactam on the edge of GO and then coupled 4,4'-methylenebis(phenylisocyanate) for preparation of the GO precursor [30]. Yadav et al. click coupled poly(ε-caprolactone) to the graphene nanoplatelets from the edge carboxyl groups converted into alkynyl [31]. Polyvinyl alcohol coupled GO was also synthesized by Salavagione et al. using grafting onto esterification reaction [32]. By combination of atom transfer nitroxide radical coupling (ATNRC) with the grafting onto strategy, an efficient way to functionalize graphene nanoplatelets with presynthesized PNIPAAm was obtained by Deng et al. [13]. TEMPO-functionalized graphene nanoplatelets from the edge reacted with Br-terminated PNIPAAm homopolymer presynthesized by SET–LRP to form PNIPAAm-graphene sheets nanocomposite in which the polymers were covalently linked onto the graphene via the alkoxyamine conjunction points.

In this study, we established a well-defined process to attach polystyrene chains with various graft densities at the edge of GO nanoplatelets. Therefore, we synthesized a bifunctional modifier with ATRP initiator and hydroxyl moieties which can easily reaction with edge carboxylic groups of GO by an esterification reaction. Subsequently, ATRP of styrene in the presence of functionalized graphene nanoplatelets has been carried out. Polystyrene chains are grown from the edge of graphene nanoplatelets by a grafting from reaction. Attachment of ATRP initiator and polystyrene to the edge of graphene nanoplatelets and effect of graft density on the

6

kinetics, structure, and also thermal properties of the nanocomposites are fully investigated. Designation of the samples with various type of their filler are summarized in Table 1.

Table 1- Designation of the samples with various graphene type and amount

Chemicals		
Designation	*Discription*	
BG	1,4-Butanediol	
BiBB	alpha-bromoisobutyryl bromide	
CBr	4-Hydroxybutyl 2-Bromopropionate	
Graphenes		
Graphene type	*Discription*	
G	Graphene	
GO	Graphene oxide	
GCBrL	Low density CBr-functionalized GO	
GCBrH	High density CBr-functionalized GO	
Nanocomposites		
Sample	*Graphene type*	*Graphene content (wt%)*
PLX	GCBrL	0.X
PHX	GCBrH	0.X
Polystyrene-functionalized graphenes		
Functionalized Graphene	*Graphene Source*	*Graphene content in the precursor (wt%)*
PLXA	GCBrL	0.X
PHXA	GCBrH	0.X

2. EXPERIMENTAL SECTION

Materials

Graphite was purchased from Merk, Germany. Styrene (Aldrich, 99%) was passed through an alumina-filled column, dried over calcium hydride, and distilled under reduced pressure (60 °C, 40mmHg). Copper(I) bromide (CuBr, Aldrich, 98%) was washed with glacial acetic acid, filtered, and finally washed with ethanol; it was dried under vacuum oven (50 °C, 40 mmHg) and then stored in a nitrogen atmosphere. N,N,N′,N″,N″-pentamethyldiethylenetriamine (PMDETA, Aldrich, 99%), ethyl alpha-bromoisobutyrate (EBiB, Aldrich, 97%), alpha-bromoisobutyryl bromide (BiBB, Aldrich, 97%), anisole (Aldrich, 99%), 1,4-butanediol (BG, Sigma-Aldrich, 99%), triethylamine (TEA, Sigma-Aldrich, 99%), N,N′-Dicyclohexylcarbodiimide (DCC, Aldrich, 99%), 4-dimethylaminopyridine (DMAP, Aldrich, 99%), Potassium permanganate (KMnO$_4$, Sigma-Aldrich, 99%), Sodium nitrate (NaNO$_3$, Sigma-Aldrich, 99%), neutral aluminum oxide (Al$_2$O$_3$, Aldrich), N,N-Dimethylformamide (DMF, Sigma, 99%), and Sulfuric acid (H$_2$SO$_4$, Merck) were used as received.

Characterization

^{1}H NMR (300 MHz) spectra were recorded on a Bruker Avance 300 spectrometer using CDCl$_3$ as the solvent and tetramethylsilane as the internal standard. A pulse delay of 1 s was used to ensure complete relaxation of spins.

Fourier transform infrared (FTIR) spectra were recorded on a Bomem FTIR spectrophotometer within a range of 500–4400 cm^{-1} using a resolution of 4 cm^{-1}. An average of 32 scans has been reported for each sample. The cell pathlength was kept constant during all the experiments. The samples were prepared on a KBr pellet in vacuum desiccators under a pressure of 0.01 torr.

X-ray photoelectron spectroscopy (XPS) was carried out on a Gammadata-Scienta Esca 200 hemispherical analyzer equipped with an Al Kα (1486.6 eV) x-ray source.

Elemental analysis (EA) was carried out with an Elementar Vario max CHNO Analyser (Hanau, German). Total carbon, hydrogen, nitrogen, and oxygen were determined by dry combustion method.

Gas chromatography (GC) is a simple and highly sensitive characterization method and does not require removal of the metal catalyst particles. GC was performed on an Agilent-6890N with a split/splitless injector and flame ionization detector (FID), using a 60 m HP-INNOWAX capillary column for the separation. The GC temperature profile included an initial steady heating at 60 °C for 10 min and a 10 °C/min ramp from 60 to 160 °C. The ratio of monomer to anisole at different stages of the reaction was measured.

The average molecular weight and molecular weight distributions were measured by gel permeation chromatography (GPC) technique. A Waters 2000 ALLIANCE with a set of three columns of pore sizes of 10000, 1000, and 500 Å was utilized to determine polymer average molecular weights and polydispersity index (PDI). THF was used as the eluent at a flow rate of 1.0 mL/min, and the calibration was carried out using low polydispersity polystyrene standards. For the GPC measurements, catalyst particles were removed by passing the polymer solutions through a neutral aluminum oxide column.

Thermal gravimetric analyses were carried out with a PL thermo-gravimetric analyzer (Polymer Laboratories, TGA 1000, UK). The thermograms were obtained from ambient temperature to 550 °C at a heating rate of 10 °C/min. A sample weight of about 10 mg was used for all the measurements, and nitrogen was used as the purging gas at a flow rate of 50 ml/min; an empty pan was used as the reference.

Thermal analysis was carried out using a differential scanning calorimetry (DSC) instrument (NETZSCH DSC 200 F3, Netzsch Co, Selb/Bavaria, Germany). Nitrogen at a rate of 50 ml/min was used as the purging gas. Aluminum pans containing 2–3 mg of the samples were sealed using the DSC sample press. The samples were heated from ambient temperature to 220 °C at a heating rate of 10 °C/min. T_g was obtained as the inflection point of the heat capacity jump.

Raman spectra were collected in the range from 3000 to 800 cm^{-1} using Bruker Dispersive Raman Spectrometer fitted with a 785 nm laser source, a CCD detector, and a confocal depth resolution of 2μm. The laser beam was focused on the sample using an optical microscope.

X-ray diffraction (XRD) spectra were collected on an X-ray diffraction instrument (Siemens D5000) with a Cu target (λ= 0.1540 nm) at room temperature. The system consists of a rotating anode generator, and operated at 35 kV and a current of 20 mA. The samples were scanned from 2 to 10° at the step scan mode, and the diffraction pattern was recorded using a scintillation counter detector. The basal spacing of the samples was calculated using the Bragg's equation.

A Vega Tescan SEM analyzer (Czech Republic) was used to evaluate the morphology of the neat and modified graphenes which were gold-coated using a sputtering coater. The specimens were prepared by coating a thin layer on a mica surface using a spin coater (Modern Technology Development Institute, Iran).

The transmission electron microscope, Philips EM 208, with an accelerating voltage of 120 kV was employed to study the morphology of the nanocomposites.

Preparation of GO and graphene from the source of graphite

GO was prepared using modified Hummers' method. 1.5 g $NaNO_3$ and 3.0 g graphite powder were poured into a 300-mL three-necked flask which was placed in an oil bath. Then, 180 mL of H_2SO_4 was added into the reactor. The mixture was stirred for 15 min in the room temperature

10

and then 9.0 g KMnO$_4$ was slowly added into the mixture till the temperature remains under 20

°C. Subsequently, temperature was increased to 35 °C and stirring was continued for 7 h. Then,

9.0 g KMnO$_4$ was added into the reactor and stirring was continued for additional 12 h at 35 °C.

The reactor content was diluted by 600 mL deionized water. 30 mL of 30% H$_2$O$_2$ was poured

into the diluted product to reduce the unreacted KMnO$_4$. After centrifugation and washing the

product with hydrochloric acid solution (1/10 with respect to water), wet GO washed three times

with distilled water till its pH reaches to about 7. Then, graphite oxide dispersion (0.1 mg/mL)

was exfoliated by water bath ultrasonication for 1 h. Finally, dried GO powder was obtained by

filtration and vacuum at 65 °C. To obtain the graphene as reference GO was reduced by

hydrazine: Yellow to brown dispersion of GO (100 mg) in water (100 mL) was ultrasonically

agitated for 3 h. The dispersion was added into a 2-necked balloon which was placed in oil bath

at 100 °C and equipped with a condenser. Then, hydrazine hydrate (1 mL) was added into the

balloon. After 24 h, a black precipitate was obtained after filtration. The filtrate was washed 5

times by distilled water (100 mL) and ethanol (100 mL). Finally, graphene nanoplatelets were

obtained by vacuum oven at 65 °C.

Synthesis of 4-Hydroxybutyl 2-Bromopropionate (CBr)

Coupling reaction between the BiBB and BG has performed as follows: BG (45. 06 g, 0.5

mol), TEA (8 ml, 0.057 mmol), and 250 ml THF was poured into 500 ml three-necked jacketed

lab reactor and left under purging with N$_2$ for 15 min. After setting the temperature at 0 °C,

BiBB (10.8 g, 0.05 mol) in 100 ml THF was added dropwise to the reactor and stirring was

continued overnight at the room temperature. The obtained liquid was separated from the solid

filtrates by filtration and then left in oven to evaporate the solvent. Then, 200 ml deionized water

was added to the obtained liquid and the final product was extracted by chloroform. Then, the

11

organic phase was separated and dried by $MgSO_4$. Distillation in vacuum yields a dark yellow liquid [33].

Functionalization of GO by CBr

Coupling reaction between the carboxyl functional groups of GO and hydroxyl groups of CBr was carried from the edge of GO using the methods reported previously [34]. GO (0.5 g) was dispersed in 150 ml DMF and after stirring for 2 h, ultrasonically agitated for 30 min to reach a homogeneous suspension. Subsequently, BiBB (2.459 g for high graft density and 0.491 g for low graft density sample) in 50 ml DMF was added to the GO dispersion dropwise and stirring was continued to reach a homogeneous solution. Subsequently, DCC (6 g, 31.30 mmol) and DMAP (0.45 g, 3.69 mmol) were added into the reactor during 20 min and left under stirring for 16 h. After addition of 50 ml DMF to the reactor content, it was filtered through a 0.2 μm PTFE filter. The filtrate was washed 4 times with 50 ml DMF to remove the unreacted CBr molecules. After drying the filtrate in oven at 60 °C, GCBrL and GCBrH were obtained.

Preparation of graphene/polystyrene nanocomposites

ATRP reactions were performed in a 150–ml lab reactor which was heated by an oil jacket thermostated at 110 °C. A number of batch polymerizations were run in a solution medium with the molar ratios of 100:0.5:1:1 for [M]:[EBiB]:[CuBr]:[PMDETA]. The reactor was degassed and back-filled with nitrogen gas three times, and then left under N_2. Batch experiments were run by adding deoxygenated monomer (styrene, 30 ml), GCBr, catalyst (CuBr, 0.188 g), ligand (PMDETA, 0.27 ml), DMF as diluent (10 ml), and 0.5 ml of deoxygenated anisole as internal standard to the reactor and then increasing the reaction temperature to 110 °C. The solution turned light green as the CuBr/PMDETA complex formed. Finally, after the majority of the metal complex had formed, free initiator (EBiB, 0.96 ml) was added to the system to start the

polymerization. A sample was taken before the reaction started and used as a reference to measure the conversion.

Separation of polystyrene-attached graphene nanoplatelets

Nanocomposites were dissolved in DMF. Then, by high-speed ultracentrifugation and passing the solution through a 0.2 mm filter, the unattached polymer chains were separated from the anchored ones via passing through the filter pores. Washing the filter in DMF and exposing the solution to the air yields polystyrene-attached graphene nanoplatelets.
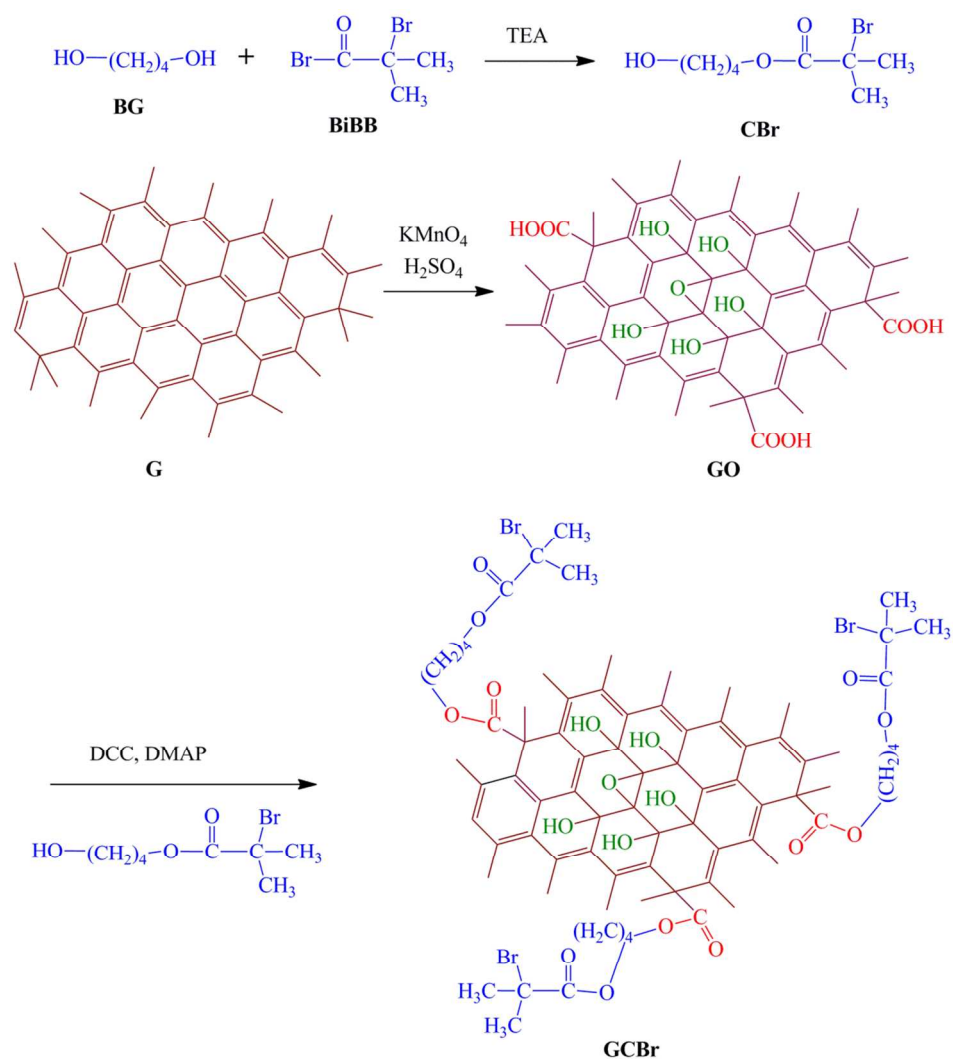
Figure 1- Graphene oxidation and subsequent functionalization with CBr

13

3. RESULTS AND DISCUSSION

Graphite was used to prepare GO by an oxidation reaction. As shown in Figure 1, Coupling reaction of 1,4-butanediol and BiBB yields CBr with functional groups of hydroxyl and ATRP initiator. Subsequently, GO was functionalized with CBr from carboxyl groups by an esterification reaction to reach edge-functionalized graphene nanoplatelets (GCBr). Finally, GCBr was used in different weight percents as the precursor for ATRP of styrene.

A. Structural Analysis
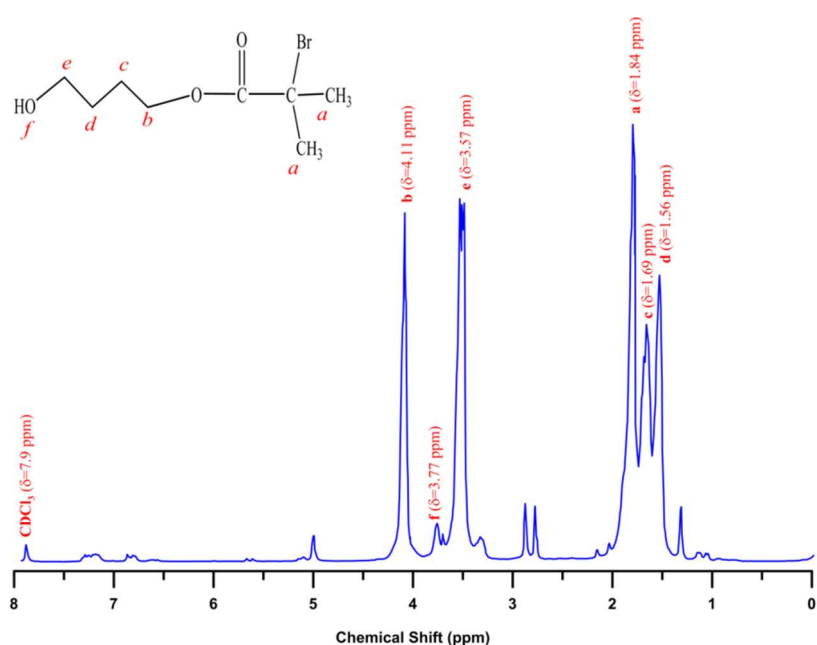
Figure 2- ^{1}H NMR spectrum of CBr

Figure 2 shows the ^{1}H NMR spectrum of the CBr modifier. The peak at δ=1.84 ppm is associated with the methyl protons adjacent to the bromine group (**a**, C–CH$_3$). Methylene group in the vicinity of ester group appeared in the chemical shifts of δ=4.11 ppm (**b**, C(O)O–CH$_2$). Peaks at δ=1.56 and 1.69 ppm correspond to the inner methelene groups of the BG moiety (**c, d**). The peak at δ=3.57 ppm is in accord with the hydroxyl adjacent methylene group (**e**, CH$_2$–OH). The peak at δ=3.77 ppm corresponds to the hydroxyl group (**f**, OH). From the calculation of peak

area at the chemical shifts of δ=4.11 and 3.57 ppm (**b** and **e**), it is revealed that 32% coupling reactions were occurred between one BG and two BiBB molecules as a side reaction. Considering the peak area at chemical shifts of δ=1.84 and 4.11 ppm (**a** and **b**), it can be concluded that the CBr synthesis efficiency is about 86% (after subtraction of coupling reaction between one BG and two BiBB molecules).

FTIR spectra of graphene, GO, CBr, GCBrL, GCBrH, polystyrene, and its nanocomposites with various graft densities are shown in Figure 3 (A) and (B). After oxidation of graphene nanoplatelets, hydroxyl stretching vibration at 3398 cm^{-1}, carboxyl stretching vibration at 1716 cm^{-1}, and carbon-oxygen vibration (C–O–C) at 853 and 1051 cm^{-1} are appeared [35]. In addition, the intensity of OH-stretching vibration observed in the wave number of 3414 cm^{-1} is increased by the oxidation of graphene. For CBr, the peaks between 2870 and 2945 cm^{-1} are assigned to the stretching vibration of C–H bonds in methyl or methylene groups [33]. The peak at 1448 cm^{-1} is attributed to the methylene C–H bending vibration and the peak at 1407 cm^{-1} may be due to the vinyl C–H in plane bending vibration of CBr [36, 37]. The two peaks at around 1322 and 1300 cm^{-1} and the peak at 1170 cm^{-1} are assigned to –C–CO–O– skeletal vibration originating from the methacryloxy groups [36]. Carboxyl stretching vibration at 1713 cm^{-1} and carbon-carbon double bond vibration at 1634 cm^{-1} are also observed in the spectra of CBr. Stretching vibration of hydroxyl groups is observed at 3380 cm^{-1}. The C–OH group reveals a peak at 1162 cm^{-1}. Also, the peak at 1387 cm^{-1} corresponds to the symmetry deformation of methyl groups in BiBB structure which confirms the attachment of ATRP initiator in GCBrL and GCBrH [38]. Also, the C–Br vibration seen at 757 cm^{-1} in GCBrL and GCBrH patterns clearly shows that modification process was carried out successfully [39]. Several characteristic peaks are observed in the FTIR spectra of polystyrene (Figure 3 (B)). The peaks at 2918 and 1607 cm^{-1} are assigned

to the CH–stretching vibration of methylene groups and stretching vibration of non-conjugated carbon–carbon double bonds respectively. Asymmetric CH–bending vibration of methylene groups causes a peak at 1455 cm^{-1}. Appearance of the C=O stretching vibration in the spectra of PH3 and PL3 shows the presence and attachment of functionalized graphenes to polystyrene chains. A characteristic bond is also seen at the wave number of 755 cm^{-1} corresponding to C–Br bond. Therefore, the chain end functionality of polystyrene synthesized via ATRP could be easily demonstrated by FTIR technique [40]. Variation of the wave number of characteristic bonds in the nanocomposites spectra clearly indicates an interaction between the phenyl ring of polystyrene chains and graphene functional groups.
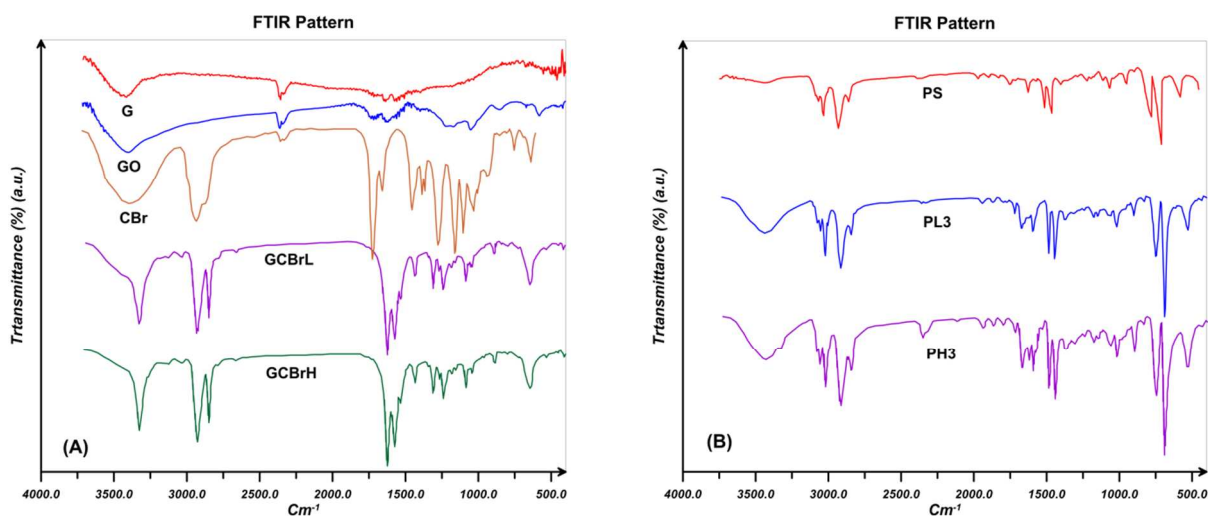
Figure 3- FTIR pattern for (A) graphene, GO, CBr, GCBrL, and GCBrH and (B) polystyrene and its nanocomposites with various graft densities

XPS was used to investigate the surface composition of the GO and GCBrH. Figure 4 (A) shows the survey data and also the higher resolution data of the Br$_{3d}$ areas. Survey-scan spectrum of GO varies from the GCBrH considerably at the binding energy of 72-80 eV which relates to the Br atom. Appearance of Br$_{3d}$ band in the spectrum of GCBrH originates from the covalent

attachment of CBr on the edge of GO nanoplatelets [11]. In addition, increase of C/O vale from

0.72to 1.13 shows that functionalization of GO by CBr results in the partial reduction of GO

nanoplatelets. For more clarification, EA results were also accompanied in Table 3.

   As shown in the Figure 4 (B), the C_{1s} band spectra at the binding energy of 282–292 eV is used

to evaluate the variation of various functional groups content in GO and GCBrH. The lower peak

area of the C_{1s} spectra of the GO shows that its degree of oxidation of is higher. According to the

literature, oxygen containing functional groups of carbonyl (C=O), carboxyl (O–C=O), epoxide

(O–C–O), and hydroxyl (–COH) are formed upon the oxidation of graphene [2, 41-42].

   Figure 4 (C) shows that the same oxygen functional groups are still present in GCBrH and

initiator moieties are successfully attached to the carboxyl groups by appearance of C–Br peak at

the binding energy of 287.1 eV [41, 43]. The numerical results of XPS in the case of GO

functional groups [42] and GCBrH are presented in Table 2. According to the results, increasing

C=C peak and reduction of carbonyl and carboxyl peaks the intensities by the functionalization

process show that the reaction conditions cause a slight reduction of the oxide functionalities on

the structure of GO [2, 43]. The reduction of oxygen containing functional groups by the

modification process was also revealed by the results of elemental analysis which confirms the

reduction of GO nanoplatelets upon the modification reactions. Carbon-oxygen ratio in GO from

the both XPS and EA results is lower than unity which shows the high amount of oxidation

during the Hummer method. Carbon and Br ratio of 21.92 from the XPS results shows that about

1 molecule CBr was attached to every 3.65 aromatic ring of GCBrH. The grafting ratio of CBr

modifier was calculated to be 6.23% via the data of Br content. From the decomposition of C_{1s}

signal into various groups in Figure 4 (C), relative atomic percentages are extracted and

presented in Table 2. Br 3d core-level spectra for GCBrH around the binding energy of 70-72 eV

17

can be curve-fitted with two peak components having binding energies at about 70 (Br3d$_{5/2}$) and

71.8 eV (Br3d$_{3/2}$) [43]. The reduction of oxygen containing functional groups in combination

with the increase of graphitic carbon bonds also confirms the partial reduction of GO

nanoplatelets by the modification process.
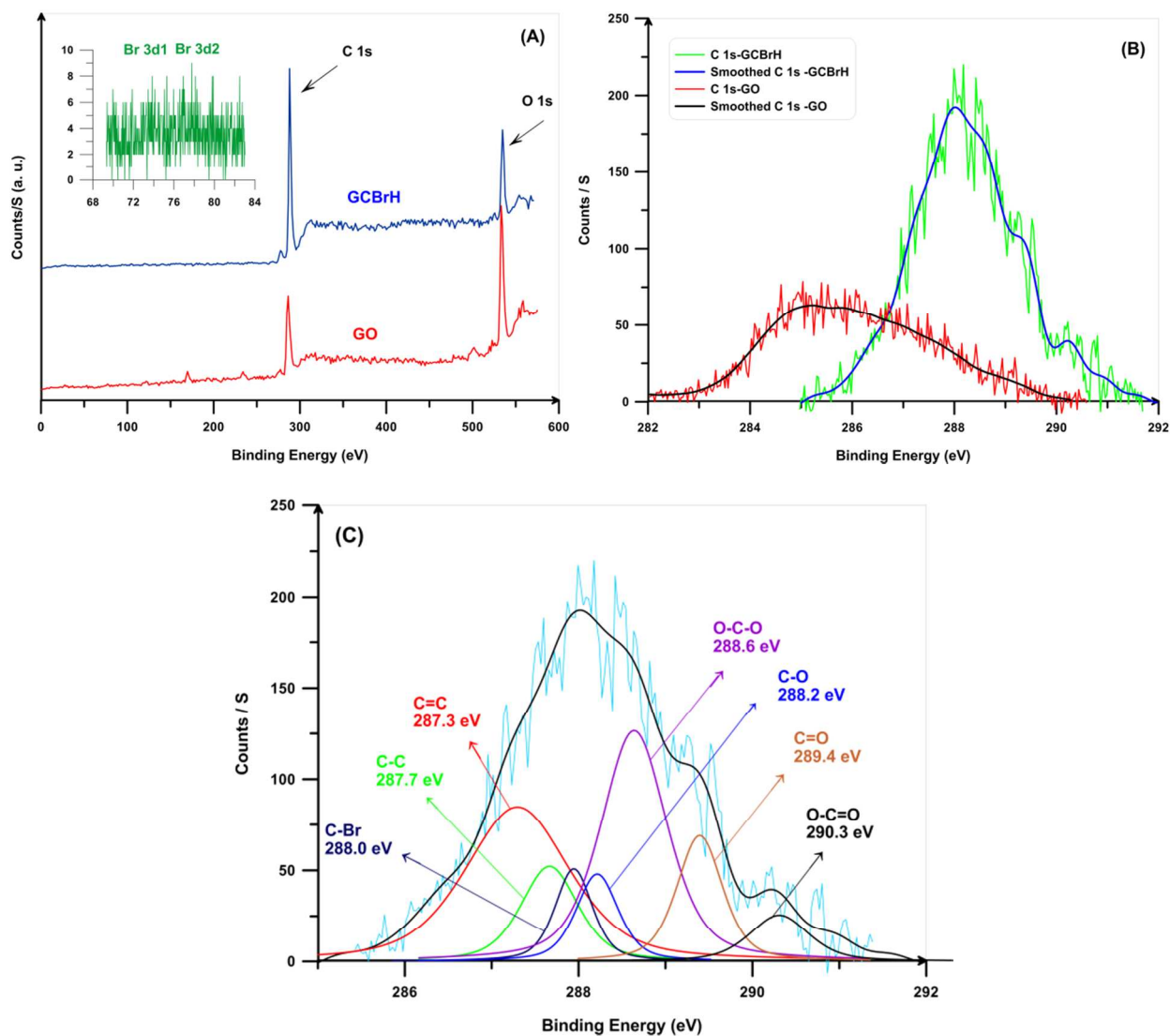
Figure 4- (A) Wide scan XPS for GO and DCBrH, (B) C1s core-level spectrum for GO and

DCBrH, and (C) deconvoluted C1s core-level spectrum of DCBrH

Table 2- Elemental surface composition of GO and GCBrH resulted from determined by XPS and surface functional group compositions obtained from the decomposition of the C1s signal

Graphene type	Composition (%)			Ratio	
	O	**C**	**Br**	**C/O**	**C/Br**
GO	58.07	41.93	----	0.72	----
GOHBrH	45.67	51.96	2.37	1.13	21.92
	Composition of C in groups						
	O=C–O	**C=O**	**C–O–C**	**C=C**	**C–O**	**C–C**	**C-Br**
GO	5.72	30.47	24.9	21.23	8.99	8.69	----
GOHBrH	9.87	11.68	23.49	27.92	9.05	9.97	8.02

Table 3- Elemental composition of G, GO, GCBrL, and GCBrH resulted from Elemental Analysis

Graphene type	Element			
	C	**H**	**O**	**C/O**
G (atom%)	95.3	1.8	2.9	32.86
GO (atom%)	39.7	2.4	57.9	0.69
GCBrL (atom%)	49.6	4.1	45.2	1.09
GCBrH (atom%)	52.7	5.1	40.4	1.30

Figure 5 displays the GPC traces for the free and graphene-attached polystyrene chains. Polymer chain characterizations in terms of number and weight average molecular weights and polydispersity indices derived from GPC traces in addition to conversion values are also summarized in Table 4. Higher conversion values for the graphene containing experiments show the acceleration effect of graphene on the polymerization rate. A large number of remained

oxygen containing functional groups on the surface of GO after modification with CBr seems to apply a polarizing effect into the polymerization medium and therefore increase the rate of polymerization. As reported previously, polar solvents (especially hydroxyl containing ones like water, phenol, and carboxylic acids) exert a rate acceleration effect on the polymerization systems for rising radical activation rate and reducing radical recombination rate [44-48]. Additionally, negatively charged surface could possibly absorb positively charged catalyst (Cu ions at our work) and consequently enhances the chain growth rate [49]. The accelerating effect of other nanofillers with oxygen containing functional groups on the polymerization rate was also reported in other works [50, 51]. As it is clear, addition of functionalized GO into the polymerization medium results in the free and attached polystyrene chains with various characteristics. The amount of anchored initiator increased in the reaction medium by addition of graphene content; therefore, molecular weights of both the free and attached chains decrease. However, because of the effect of neighbor active heads which is known as viscose region, attached chains have greater molecular weights. Behling and coworkers [52] show that a large number of dormant chains are present in the viscose region near the surface. This non-homogeneity result in the rapid diffusion of small activator species compared with the deactivator molecules. Therefore, higher concentration of activator in this region results in higher activation and finally higher polymerization rate. Thus, attached polystyrene chains possess higher molecular weights. By increasing grafting density, this effect would be magnified and results in extra increase of molecular weight and conversion values. Addition of graphene content and grafting density which results in higher initiator moieties in the reaction medium, certainly results in higher PDI values of attached and free chains. However, PDI values of attached chains are higher than the free ones. This may rise from the small distance between the

growing radicals in the attached form which in turn facilitates the combination of growing radicals. Increasing PDI values of polymer chains in the presence of various nanofillers was reported frequently [53-55]. In addition, graphene as an impurity in the polymerization system causes the molecular weight distribution of the resultant polymers to be broadened. For free chains which propagate in much lower rates, decrease of molecular weight is observed by increase of graphene content and also grafting density. However, PDI values of free chains are lower than the attached polystyrene chains.

21
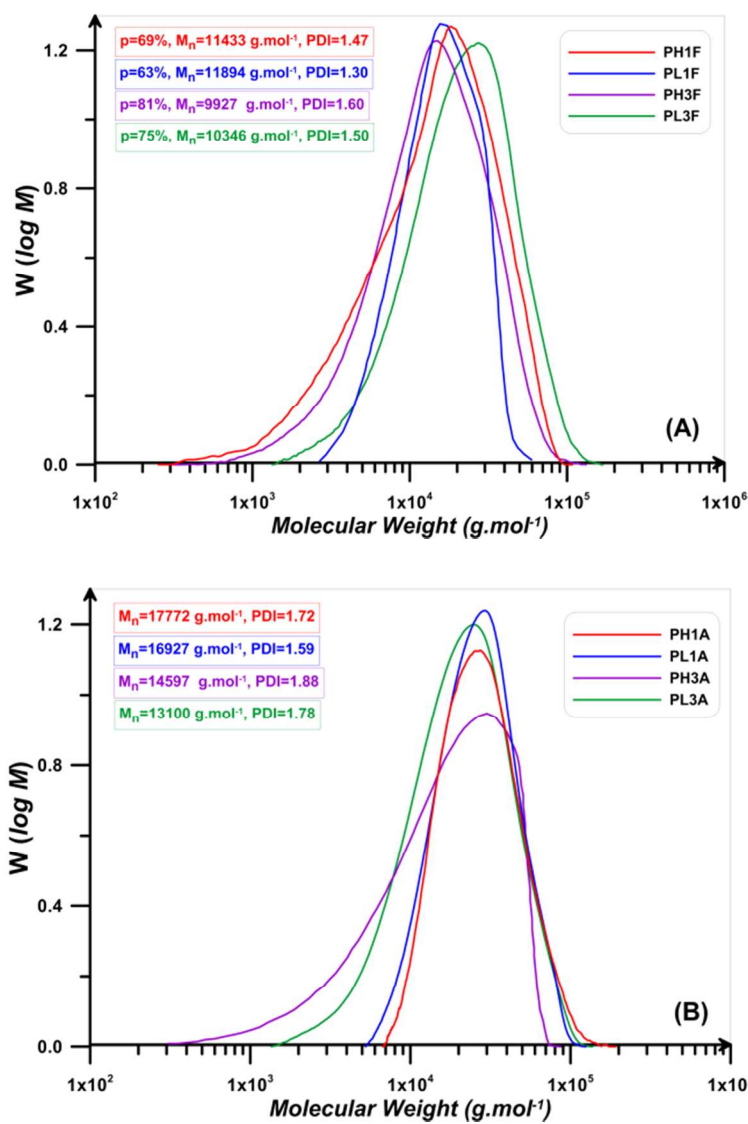
Figure 5- GPC traces for the (A) free and (B) graphene-attached polystyrene chains

Table 4- Kinetic data for the free and graphene-attached polystyrene chains

Sample	Reaction Time (h)	Conversion	M_n (mol.g^{-1})		PDI	
			Free	Attached	Free	Attached
PS	5	65.2	12680	----	1.10	----
PH1	5	69.4	11433	17772	1.47	1.72
PH2	5	72.1	10710	16257	1.52	1.83
PH3	5	81.9	9927	14597	1.60	1.88
PH4	5	85.2	7525	12542	1.55	1.93
PL1	5	63.3	11894	16927	1.30	1.59
PL2	5	70.7	10925	15154	1.37	1.65
PL3	5	75.5	10346	13100	1.50	1.78
PL4	5	79.2	7914	12115	1.53	1.85

B. Thermal Analysis

Thermal stability of the samples is studied by TGA. Figure 6 (A) illustrates TGA thermograms of weight loss as a function of temperature for the neat and modified graphenes. GO stores some water in its π-stacked structure and therefore shows some mass loss below 100 °C [56]. By substitution of CBr modifier with the edge polar oxygen groups in GCBrL and GcBrH, the extent of the absorbed water decreases. According to the results, pristine graphene reaches to 93.2 wt% char value at 600 °C. GO thermogram shows major weight losses between 150 and 220 °C, which corresponds to CO, CO_2, and steem release from the most labile functional groups. Between 230 and 600 °C, a slower mass loss is observed which can be attributed to the degradation of more stable oxygen functionalities [57, 58]. However, a different decomposition

22

pattern was observed after the functionalization of GO with CBr. This can be explained by the loss of oxygen-containing functional groups at the edge during the reaction between carboxyl functionalities of graphene oxide and CBr. The char value of 44.7 and 47.3% in GCBrH and GCBrL thermogram up to 550 °C is due to the degradation of its modifier and the remained oxygen-containing functional groups. Discrepancies between the weight loss of GO and modified graphenes (4.8 and 7.4% for GCBrL and GCBrH respectively) can be a rough estimation of modifier content. Also, decomposition temperature of GO is lower than the two modified graphenes which shows that CBr modifier retards the decomposition of GO by decreasing the amount of oxygen containing functional groups.
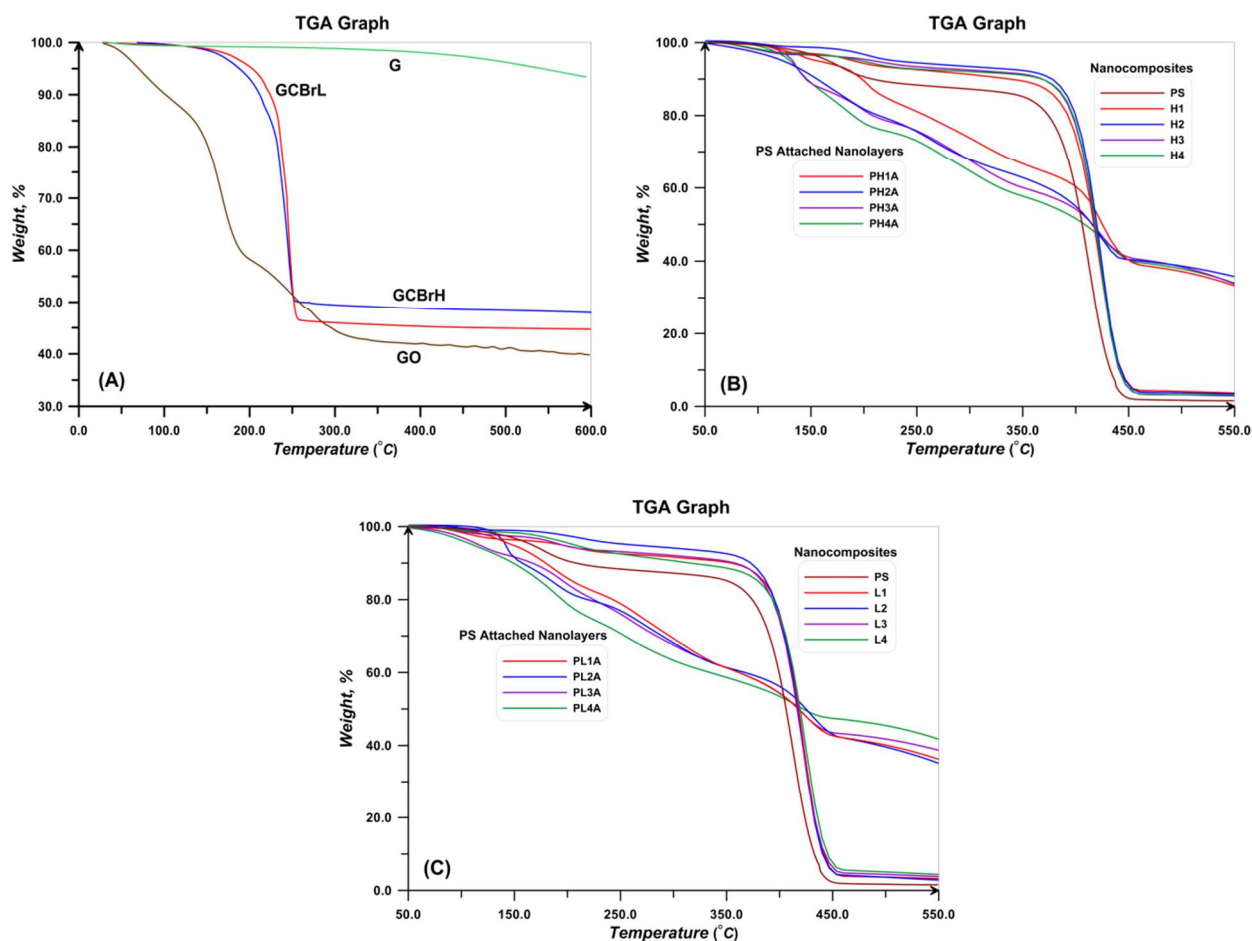
Figure 6- TGA thermograms for (A) neat and modified graphenes, (B) nanocomposites with low graft density, and (C) nanocomposites with high graft density

Figure 6 (B and C) show the TGA curves for the low and high density nanocomposites along with the corresponding graphene-attached polystyrene chains. According to the results, thermal stabilities of all the nanocomposites are higher than the neat polystyrene. The data derived from TGA thermograms (Table 5) shows char values for the nanocomposites and polystyrene-attached graphene nanoplatelets along with the weight loss at the third degradation step of polystyrene-attached nanoplatelets. In the case of nancomposites, degradation temperature is lower for lower graphene contents. Degradation pattern of the graphene-attached polystyrene chains are consist of three separate steps. The first two steps relate to decomposition of oxygen containing functional groups of graphene layers; however, the third step relates to the attached polystyrene chain degradation. Graphenes with higher graft densities exhibits lower amount of char value since their degradable polystyrene chains are higher than the graphenes with lower graft densities. Decreasing of the degradation value at the third step by addition of graphene content is very low and originates from the grafted polystyrene chains with lower molecular weights. Char values of the nanocomposite are much lower than the polystyrene-attached graphene layers and increases by increasing graphene content. Degradation temperatures of the nanocomposites are also higher in the case of higher graft contents.

The weight and molar ratio of CBr and polystyrene chains on the graphene layers can be estimated from TGA thermograms. Equations 1 and 2 are used to calculate these parametes [59–62].

$$G_{r,MPS} \left(weight\ ratio\ of\ MPS\ on\ graphene \right) = \frac{w\%_{MPS}}{100 - w\%_{MPS}} \tag{1}$$

$$G_{r,PS}\left(weight\ ratio\ of\ PS\ on\ graphene\right) = \frac{w\%_{PS}}{100 - w\%_{PS}} - \frac{w\%_{MPS}}{100 - w\%_{MPS}} \tag{2}$$

Table 5- Data derived from the TGA thermograms

Sample	GCBrL	GCBrH	PL1A	PH1A	PL2A	PH2A	PL3A	PH3A	PL4A	PH4A
Char value	44.7	48.3	42.3	34.4	39.5	36.1	36.5	34.1	35.4	34.0
Third step degradation	4.8	7.4	18.1	21.9	16.9	21.1	14.7	19.5	13.8	18.2
$G_{r,CBr} \times 10^2$	5.04	7.99	---	---	---	---	---	---	---	---
$G_{r,PS} \times 10^2$	---	---	17.06	20.05	15.29	18.88	12.19	16.23	10.97	14.26

DSC in the temperature range of 70–110 °C was employed to study the effect of graphene nanoplatelets and also graft density on the relaxation behavior of polystyrene chains. Glass transition as a macroscopic indication for relaxation of polystyrene chains was obtained after removing the thermal history. Figure 7 shows the DSC thermograms and corresponding T_g values for the neat polystyrene and its nanocomposites with various graft contents. The nature of interface between the substrate and polymer chains is an important factor in determination of T_g values [63]. Graft polymer chains relax in a different manner in comparison with the free chains [5, 6]. Confinement of substrates commonly increases T_g value. Some other parameters such as molecular weight and its distribution can also affect the relaxation and therefore T_g value [6, 7, 64]. In graphene loaded nanocomposites, polarity of the host polymer can remarkably increase T_g value. About 40 °C increase in the T_g of polyacrylonitrile by addition of only 1 wt% of graphene oxide was ascribed to the strong interaction between GO and polyacrylonitrile chains

25

[65]. In graft polystyrene systems, length of polymer chain, density of grafting, size of substrate, and loading value can also affect the T_g value [6]. However, addition of graphene results in lower variation of T_g value in comparison with the polar polymers. According to the results, high graft density nanocomposites show a higher increase of T_g by the addition of graphene content (20.8 against 20.2 °C). T_g of the high graft density nanocomposites is higher and it is increased with adding graphene content. Addition of GCBr decreases the molecular weight of free polystyrene chains. Polystyrene chains are more confined by increasing their population on graphene nanoplatelets. Interaction between the free and attached polystyrene chains results in higher T_g values and this interaction becomes more strong by increasing the amount of anchored chains. About 21 °C increase of T_g value by the addition of only 0.4 wt% graphene shows that nanoplatelets exerts more confinement on the relaxation behavior of polystyrene chains in comparison with the other commonly used nanofillers at the same loading value [7].
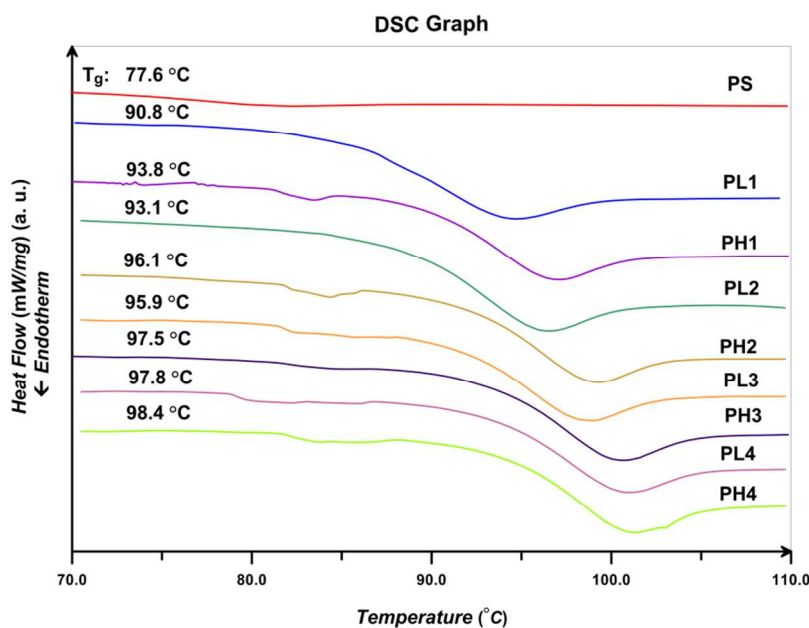
Figure 7- DSC thermograms of the neat polystyrene and its nanocomposites

C. Morphological Analysis

Ordered and disordered crystal structure of carbon in the pristine and surface-modified graphenes was studied by Raman spectroscopy (Figure 8). Three characteristics peaks at 1313 (D band), 1577 (G band), and 2641 cm^{-1} (2D or G' band) are seen in the graphene spectrum. D band (breathing mode of κ-point phonons of A_{1g} symmetry) arises from defects inherent in the graphene and the edge effect of graphene crystallites [6]. G peak (in-plane bond stretching motion of the sp^2 C atoms, E_{2g} mode) is ascribed to the aromatic domains [66, 67]. The 2D band (G' band) originates from the stacking order of the nanoplatelets [68]. The D band adsorption indicates the presence of defects. Such disorder is also reflected in the broadened and blue-shifted (higher frequency) G bands for the GO and various types of functionalized graphenes [5]. As exhibited in Figure 8, the G band of GO appeared at 1599 cm^{-1}, which is higher than that of the pristine graphene. However, after functionalization of GO, the vibration frequency of G band shifts back to the values close to the pristine graphene G band (about 1590.4 cm^{-1} for all the BiBB- and polystyrene-functionalized graphenes). This shows that the electric conjugation within the graphitic network is restored to some extent after grafting of initiator or polystyrene chains [69]. A similar phenomenon was observed by Kudin et al. who attributed this to the effect of defects and isolated double bonds [67]. The ratio of the D to G band intensities (I_D/I_G) is reciprocally related to the crystallite size [5, 70]. Oxidation and further functionalization of graphene nanoplatelets result in higher I_D/I_G. Inceasing of I_D/I_G indicates size reduction of graphitic crystallites upon mechanochemical cracking and edge distortion [68, 71]. The 2D band can be used to distinguish between the monolayer graphene, multilayer graphene, and bulk graphite. It is symmetrical for monolayer graphene, but has a shoulder in the case of graphite. Depending on the number of layers, an intermediate shape is obtained for the multilayer graphene nanoplatelets [72, 73]. Defects on the graphene basal plane can results in the

broadening of the 2D peak and appearance of the combination mode around 2600 cm^{-1} [74]. Disappearance of the 2D peak in the pattern of the functionalized graphenes shows that stacking order is diminished and exfoliated state is achieved.
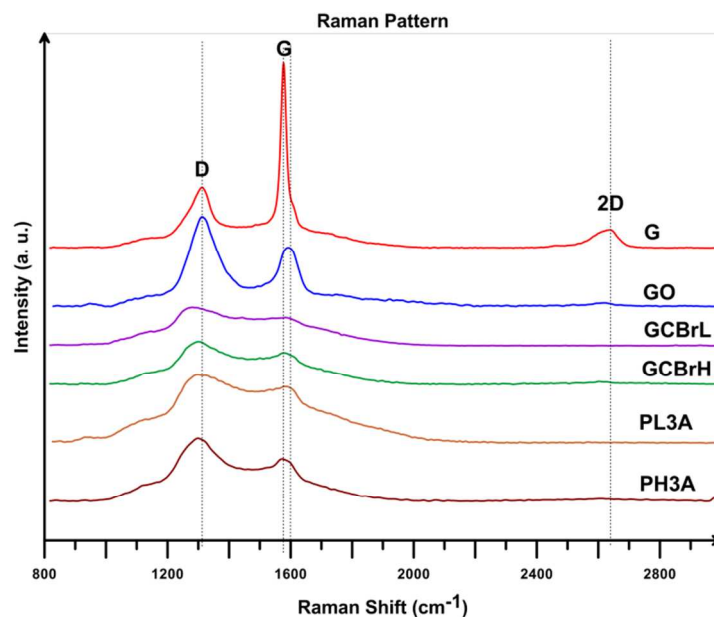
Figure 8- Raman spectra for graphene, GO, and various graft densities CBr- and polystyrene-functionalized graphenes

XRD is an effective technique for determination of the extent of graphene dispersion in a polymer matrix. Figure 9 (A) and (B) display XRD patterns of graphene, GO, BiBB anchored graphenes, and polystyrene nanocomposites with various graft densities. The interlayer distance of graphene nanoplatelets increases from 0.34 to 0.94 nm corresponding to the decrease of diffraction angle from 26 to 9.45° by the appearance of oxygen containing functional groups upon the oxidation process. The diffraction angle of about 7.49° for the BiBB-functionalized graphenes shows that increasing the interlayer distance by exerting the functional groups. The same diffraction angle for the high and low graft densities shows that attachment of higher modifier moieties from the edges cannot expand the interlayer gallery more. In addition,

28

decrease of the intensity of GO diffraction peak by the functionalization process clarifies that BiBB-functionalized graphenes expanded to some extent by intercalation of the functional groups. Also, the intensity of this peak decreases by increasing graft density which clearly shows the attachment of more modifier moieties. Disappearance of the diffraction peaks at 7.49 and 6.8° in nanocomposites with low and high grafting densities shows that graphene layers have been pushed apart and formed exfoliated structures. However, all the nanocomposites exhibit a broad amorphous shallow diffraction peak which indicates that they are purely amorphous and also graphene nanoplatelets are exfoliated and dispersed uniquely in the matrix [75]. In the exfoliated structure, the distances between the graphene nanoplatelets are so far that layers cannot give a coherent wide-angle XRD signal at diffraction angles of higher than 2° [76, 77]. Polymerization starts from the initiator moieties on the edge of graphene nanoplatelets and by propagation of polystyrene chains on the edges, graphene nanoplatelets can be pushed apart and form exfoliated structure. There is not any remarkable difference between diffraction patterns of nanocomposites with various graft densities; this shows that exertion of only a small amount of polystyrene chains can increase the interlayer distance.
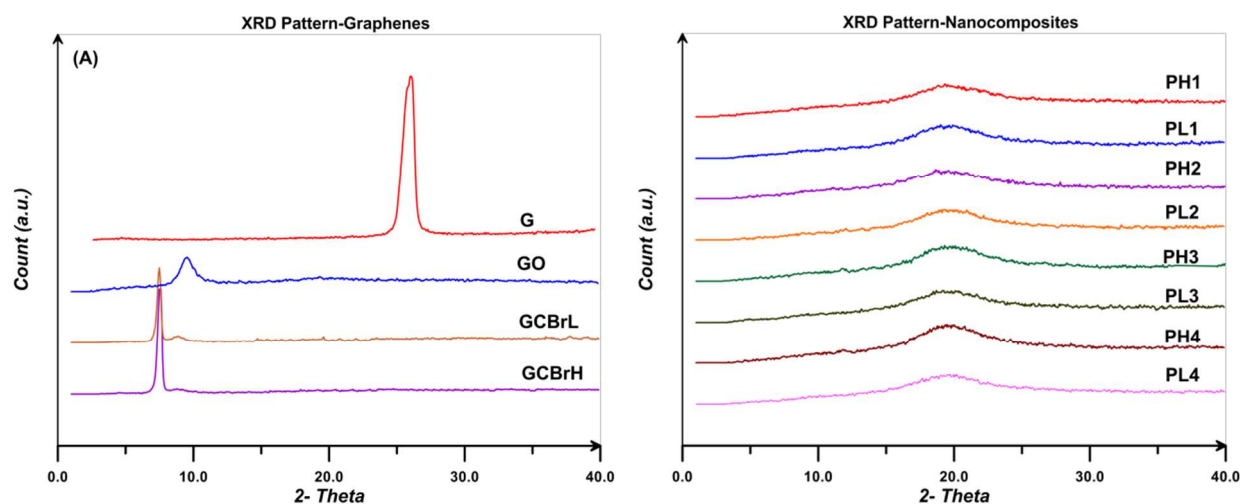
Figure 9- XRD pattern for (A) graphene, GO, GCBrL, and GCBrH and (B) nanocomposites with various graft densities

Figure 10 displays SEM images for graphene, GO, GCBrH, and PH3A respectively. Bare and flat surface of graphene nanoplatelets without any curvature is clearly observed in Figure 10 (A). Sever oxidation steps in the preparation of GO results in packed nanoplatelets as seen in Figure 10 (B). These oxygen-containing functional groups result in roughness of graphene nanoplatelets. In overall, flat and smooth morphology of graphene nanoplatelets disturbed in the oxidation and other processes needed for functionalization; therefore wrinkled layers with curvature are obtained. Also, surface area of the nanoplatelets decreases during these processes. Polystyrene coated nanoplatelets are opaque and their curvature can easily be observed in Figure 10 (C).
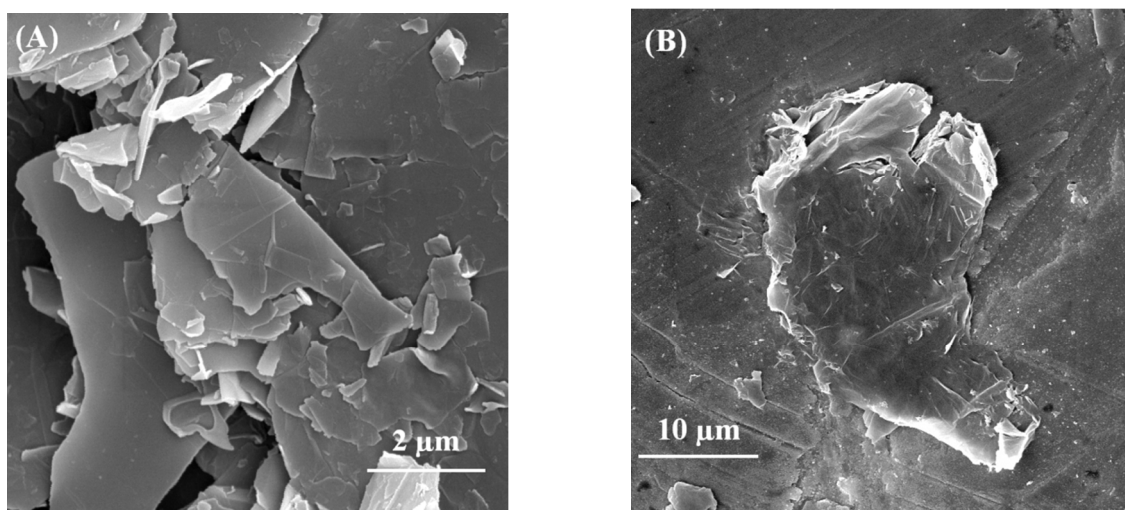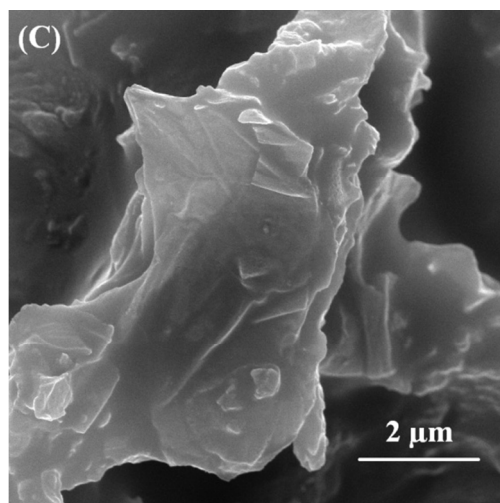
Figure 10- SEM images for (A) graphene, (B) GO, and (C) PH3A

TEM micrographs of graphene, GO, and PH3A are shown in Figure 11. Morphology of graphene nanoplatelets varies after oxidation and functionalization by polystyrene chains. Size of individual nanosheets of various graphenes extends from several hundred nanometers to ten micrometers. Pristine graphene has more transparent contrast in comparison with the nanoplatelets after oxidation and functionalization. Graphene nanoplatelets are wrinkled after oxidation because of the presence of polar oxygen containing functional groups. Lots of creases and folding are observed for GO which seems as an exfoliated crumpled thin flake. Also, surface of GO is relatively smooth and shows no other impurities. The polystyrene-attached graphene nanoplatelets (PH3A) are less transparent. All the results from TEM images show that introduction of polystyrene segments to the edge of GO was carried out successfully and polystyrene-functionalized GO nanoplatelets have monolayer structure.
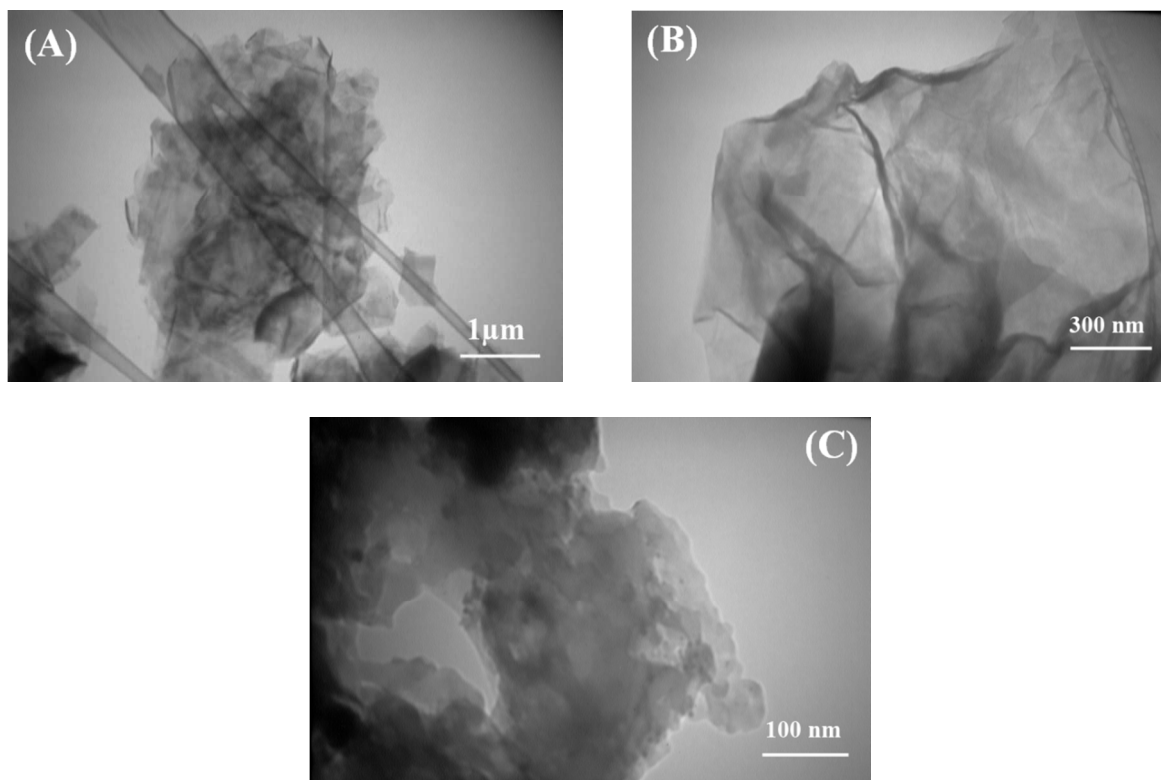
Figure 11- TEM micrograph of (A) graphene and (B) GO, and (C) PH3A

4. CONCLUSIONS

Graphite was used to prepare GO by an oxidation reaction. A bifunctional modifier (CBr) with ATRP initiator and hydroxyl moieties were synthesized by coupling reaction of 1,4-butanediol and BiBB. Then, GO was functionalized with CBr from carboxyl groups by an esterification reaction to reach edge-functionalized graphene nanoplatelets. Subsequently, ATRP of styrene in the presence of GCBr with different weight percents has been carried to evaluate the effect of graphene loading and graft density on the properties of the final product. A peak at δ=4.11 ppm in the ^{1}H NMR spectrum of CBr is associated with the methylene adjacent to the C(O)–O groups and shows the successful coupling reaction. Appearance of BiBB methyl groups deformation at 1387 cm^{-1} and C–Br vibration at 757 cm^{-1} in FTIR spectra confirms the attachment of ATRP initiator to the edge of GO. Carbon and bromine ratio of 21.92 from the XPS results shows that

about 1 molecule CBr was attached to every 3.65 aromatic ring of GCBrH. The grafting ratio of CBr modifier was calculated to be 6.23% via the data of bromine content. Molecular weights of attached polystyrene chains are higher. By increasing grafting density, molecular weight and conversion values increase. Addition of graphene content and grafting density results in higher PDI values of attached and free chains. However, PDI values of attached chains are higher than the free ones. TGA shows that modifier content is 4.8 and 7.4% in GCBrL and GCBrH respectively. Graphenes with higher density of graft polystyrene show greater degradation at the third step. Also, the intensity of third step decreases by the addition of graphene as a result of decreasing molecular weights. T_g of the low graft density nanocomposites is higher and this discrepancy is increased with increasing graphene content. After functionalization of GO, Raman vibration frequency of G band shifts back to the values close to the pristine graphene. The difference between the I_D/I_G ratios of the GO and various kinds of functionalized graphenes shows that covalent bonds between graphene and initiator moieties have been formed successfully. The same X-ray diffraction angle for the various graft densities at 7.5° shows that attachment of higher modifier moieties from the edges cannot expand the interlayer gallery anymore. Disappearance of diffraction peaks in the nanocomposite patterns shows that graphene nanoplatelets have been pushed apart and formed exfoliated structure. Flat and smooth morphology of graphene nanoplatelets varies in the oxidation and other functionalization processes and therefore wrinkled nanoplatelets with curvature are obtained. All the results from TEM images show that introduction of polystyrene segments to the edge of GO was carried out successfully and polystyrene-functionalized GO nanoplatelets have uniform polymer coating.

ACKNOWLEDGMENTS

REFERENCES

(1)   H. Roghani-Mamaqani, V. Haddadi-Asl, M. Salami-Kalajahi, *Polym. Rev.*, 2012, **52**, 142–188.

(2)   S. H. Lee, D. R. Dreyer, J. An, A. Velamakanni, R. D. Piner, S. Park, Y. Zhu, S. O. Kim, C. W. Bielawski, R. S. Ruoff, *Macromol. Rapid. Commun.*, 2010, **31**, 281–288.

(3)   Y. Deng, J. Z. Zhang, Y. Li, J. Hu, D. Yang, X. Huang, *J. Polym. Sci.: Part A: Polym. Chem.*, 2012, **50**, 4451–4458.

(4)   G. Goncalves, P. A. A. P. Marques, A. Barros-Timmons, I. Bdkin, M. K. Singh, N. Emami, J. Gracio, *J. Mater. Chem.*, 2010, **20**, 9927–9934.

(5)   M. Fang, K. Wang, H. Lu, Y. Yang, S. Nutt, *J. Mater. Chem.*, 2009, **19**, 7098–7105.

(6)   M. Fang, K. Wang, H. Lu, Y. Yang, S. Nutt, *J. Mater. Chem.*, 2010, **20**, 1982–1992.

(7)   H. Roghani-Mamaqani, V. Haddadi-Asl, M. Najafi, M. Salami-Kalajahi, *AIChE J.*, 2011, **57**, 1873–1881.

(8)   H. Roghani-Mamaqani, V. Haddadi-Asl, M. Najafi, M. Salami-Kalajahi, *J. Appl. Polym. Sci.*, 2012, **123**, 409–417.

(9)   M. Salami-Kalajahi, V. Haddadi-Asl, F. Behboodi-Sadabad, S. Rahimi-Razin, H. Roghani-Mamaqani, *Polym. Composites*, 2012, **33**, 215–224.

(10) L. Ahmadian-Alam, V. Haddadi-Asl, H. Roghani-Mamaqani, L. Hatami, M. Salami-Kalajahi, *J. Polym. Res.*, 2012, **19**, 9773.

(11) S. Rahimi-Razin, V. Haddadi-Asl, M. Salami-Kalajahi, F. Behboodi-Sadabad, H. Roghani-Mamaqani, *Int. J. Chem. Kinet.*, 2012, **44**, 555–569.

(12) Y. Tan, L. Fang, J. Xiao, Y. Song, Q. Zheng, *Polym. Chem.*, 2013, **4**, 2939–2944.

(13) Y. Deng, Y. J. Li, J. Dai, M. Lang, X. Huang, *J. Polym. Sci.: Part A: Polym. Chem.*, 2011, **49**, 1582–1590.

(14) Z. Jin, T. P. McNicholas, C. J. Shih, Q. H. Wang, G. L. C. Paulus, A. J. Hilmer, S. Shimizu, M. S. Strano, *Chem. Mater.*, 2011, **23**, 3362–3370.

(15) Z. Liu, J. T. Robinson, X. Sun, H. Dai, *J. Am. Chem. Soc.*, 2008, **130**, 10876–10877.

(16) D. Yu, L. Dai, *J. Phys. Chem. Lett.*, 2010, **1**, 467–470.

(17) L. Kan, Z. Xu, C. Gao, *Macromolecules*, 2011, **44**, 444–452.

(18) K. P. Loh, Q. Bao, P. K. Ang, J. Yang, *J. Mater. Chem.*, 2010, **20**, 2277–2289.

(19) D. R. Dreyer, S. Park, C. W. Bielawski, R. S. Ruoff, *Chem. Soc. Rev.*, 2010, **39**, 228–240.

(20) Z. Spitalsky, D. Tasis, K. Papagelis, C. Galiotis, *Prog. Polym. Sci.*, 2010, **35**, 357–401.

(21) D. Tasis, N. Tagmatarchis, A. Bianco, M. Prato, *Chem. Rev.*, 2006, **106**, 1105−36.

(22) W. A. Braunecker, K. Matyjaszewski, *Prog. Polym. Sci.*, 2007, **32**, 93–146.

(23) S. Zhu, J. Li, Y. Chen, Z. Chen, C. Chen, Y. Li, Z. Cui, D. Zhang, *J. Nanopart. Res.*, 2012, **14**, 1132.

(24) C. Bao, Y. Guo, L. Song, Y. Kan, X. Qian, Y. Hu, *J. Mater. Chem.*, 2011, **21**, 13290–13298.

(25) C. Bao, Y. Guo, B. Yuan, Y. Hu, L. Song, *J. Mater. Chem.*, 2012, **22**, 23057–23063.

(26) Y. Lin, J. Jin, M. Song, *J. Mater. Chem.*, 2011, **21**, 3455–3461.

(27) Y. Deng, Y. Li, J. Dai, M. Lang, X. Huang, *J. Polym. Sci. Part A: Polym. Chem.*, 2011, **49**, 4747–4755.

(28) L. Ren, X. Wang, S. Guo, T. Liu, *J. Nanopart. Res.*, 2011, **13**, 6389–6396.

(29) Y. Yang, J. Wang, J. Zhang, J. Liu, X. Yang, H. Zhao, *Langmuir*, 2009, **25**, 11808–11814.

(30) X. Zhang, X. Fan, H. Li, C. Yan, S. K. Yadav, H. J. Yoo, J. W. Cho, *J. Mater. Chem.*, 2012, **22**, 24081–24091.

(31) S. K. Yadav, H. J. Yoo, J. W. Cho, *J. Polym. Sci. Part B: Polym. Phys.*, 2013, **51**, 39–47.

(32) H. J. Salavagione, M. A. Gomez, G. Martınez, *Macromolecules*, 2009, **42**, 6331–6334.

(33) C. Y. Hong, Y. Z. You, C. Y. Pan, *Chem. Mater.*, 2005, **17**, 2247–2254.

(34) Y. Pan, H. Bao, N. G. Sahoo, T. Wu, L. Li, *Adv. Func. Mater.*, 2011, **21**, 2754.

(35) H. Yang, F. Li, C. Shan, D. Han, Q. Zhang, L. Niu, A. Ivaska, *J. Mater. Chem.*, 2009, **19**, 4632–4638.

(36) V. G. Ngo, C. Bressy, C. Leroux, A. Margaillan, *Polymer*, 2009, **50**, 3095–3102.

(37) I. A. Siddiquey, E. Ukaji, T. Furusawa, M. Sato, N. Suzuki, *Mater. Chem. Phys.*, 2007, **105**, 162–168.

(38) Y. Chen, C. Wang, J. Chen, X. Liu, Z. Tong, *J. Polym. Sci.: Part A, Polym. Chem.*, 2009, **47**, 1354–1367.

(39) H. Roghani-Mamaqani, V. Haddadi-Asl, M. Najafi, M. Salami-Kalajahi, *Polym. Sci. Ser. B*, 2012, **54**, 153–160.

(40) H. Roghani-Mamaqani, V. Haddadi-Asl, M. Najafi, M. Salami-Kalajahi, *Polym. Composites*, 2010, **31**, 1829–1837.

(41) S. H. Liao, P. L. Liu, M. C. Hsiao, C. C. Teng, C. A. Wang, M. D. Ger, C. L. Chiang, *Ind. Eng. Chem. Res.*, 2012, **51**, 4573–4581.

(42) H. Roghani-Mamaqani, V. Haddadi-Asl, K. Khezri, M. Salami-Kalajahi, *Polym. Int.*, 2014; DOI: 10.1002/pi.4730

(43) Y. Chen, C. Wang, J. Chen, X. Liu, Z. Tong, *J. Polym. Sci.: Part A Polym. Chem.*, 2009, **47**, 1354–1367.

(44) X. S. Wang, S. P. Armes, *Macromolecules*, 2000, **33**, 6640–6647.

(45) U. Chatterjee, S. K. Jewrajka, B. M. Mandal, *Polymer*, 2005, **46**, 1575–1582.

(46) D. M. Haddleton, A. M. Heming, D. Kukulji, D. J. Duncalf, A. J. Shooter, *Macromolecules*, 1998, **31**, 2016–2018.

(47) X. S. Wang, N. Luo, S. K. Ying, *J. Polym. Sci. Part A: Polym. Chem.*, 1999, **37**, 1255–1263.

(48) K. Matyjaszewski, Y. Nakagawa, C. B. Jasieczek, *Macromolecules*, 1998, **31**, 1535–1541.

(49) J. N. Kizhakkedathu, D. E. Brooks, *Macromolecules*, 2003, **36**, 591–598.

(50) H. Datta, N. Singha, A. Bhowmick, *Macromolecules*, 2008, **41**, 50–57.

(51) H. Datta, N. Singha, A. Bhowmick, *J. Appl. Polym. Sci.*, 2008, **108**, 2398–2407.

(52) R. E. Behling, B. A. Williams, B. L. Staade, L. M. Wolf, E. W. Cochran, *Mocromolecules*, 2009, **42**, 1867–1872.

(53) K. Khezri, V. Haddadi-Asl, H. Roghani-Mamaqani, M. Salami-Kalajahi, *J. Polym. Res.*, 2012, **19**, 1–10.

(54) K. Khezri, V. Haddadi-Asl, H. Roghani-Mamaqani, M. Salami-Kalajahi, *J. Polym. Eng.*, 2012, **32**, 111–119.

(55) S. Rahimi-Razin, M. Salami-Kalajahi, V. Haddadi-Asl, H. Roghani-Mamaqani, *J. Polym. Res.*, 2012, **19**, 9954.

(56) Z. Sun, V. Nicolosi, D. Rickard, S. D. Bergin, D. Aherne, J. N. Coleman, *J. Phys. Chem. C*, 2008, **112**, 20264–20269.

(57) S. Stankovich, D. A. Dikin, R. D. Piner, K. A. Kohlhaas, A. Kleinhammes, Y. Jia, *Carbon*, 2007, **45**, 1558–1565.

(58) J. Shen, Y. Hu, M. Shi, X. Lu, C. Qin, C. Li, *Chem. Mater.*, 2009, **21**, 3514–3520.

(59) D. Hua, J. Tang, J. Jiang, Z. Gu, L. Dai, X. Zhu, *Mater. Chem. Phys.*, 2009, **114**, 402–406.

(60) C. H. Liu, C. Y. Pan, Polymer, 2007, **48**, 3679–3685.

(61) Y. Zhao, S. Perrier, *Macromolecules*, 2007, **40**, 9116–9124.

(62) V. G. Ngo, C. Bressy, C. Leroux, A. Margaillan, *Polymer*, 2009, **50**, 3095–102.

(63) H. Oh, P. F. Green, *Nat. Mater.*, 2009, **8**, 139–143.

(64) K. Khezri, V. Haddadi-Asl, H. Roghani-Mamaqani, M. Salami-Kalajahi, *J. Appl. Polym. Sci.*, 2012, **124**, 2278–2286.

(65) T. Ramanathan, A. A. Abdala, S. Stankovich, D. A. Dikin, M. Herrera-Alonso, R. D. Piner, D. H. Adamson, H. C. Schniepp, X. Chen, R. S. Ruoff, S. T. Nguyen, I. A. Aksay, R. K. Prud'Homme, L. C. Brinson, *Nat. Nanotechnol.*, 2008, **3**, 327.

(66) H. Hu, X. Wang, J. Wang, L. Wan, F. Liu, H. Zheng, *Chem. Phys. Lett.*, 2010, **484**, 247–253.

(67) K. N. Kudin, B. Ozbas, H. C. Schniepp, R. K. Prud'homme, A. Aksay, R. Car, *Nano. Lett.*, 2008, **8**, 36–41.

(68) I. Y. Jeon, H. J. Choi, S. M. Jung, J. M. Seo, M. J. Kim, L. Dai, *J. Am. Chem .Soc.*, 2013, **135**, 1386–1393.

(69) S. Sun, Y. Cao, J. Feng, P. Wu, *J. Mater. Chem.*, 2010, **20**, 5605–5607.

(70) J. Zhang, H. Yang, G. Shen, P. Cheng, J. Zhang, S. Guo, *Chem. Cummun.*, 2010, **46**, 1112–1114.

(71) S. Villar-Rodil, J. I. Paredes, A. M. Alonso, J. M. D. Tascón, *J. Mater. Chem.*, 2009, **19**, 3591–5393.

(72) R. Sanna, D. Sanna, V. Alzari, D. Nuvoli, S. Scognamillo, M. Piccinini, *J. Polym. Sci., Part A: Polym. Chem.*, 2012, **50**, 4110–4118.

(73) A. C. Ferrari, J. C. Meyer, V. Scardaci, C. Casiraghi, M. Lazzeri, F. Mauri, S. Piscanec, D. Jiang, K. S. Novoselov, S. Roth, A. K. Geim, *Phys. Rev. Lett.*, 2006, **97**, 187401–18744.

(74) L. Ren, T. Liu, J. Guo, S. Guo, X. Wang, W. Wang, *Nanotechnology*, 2010, **21**, 335701.

(75) M. Li, Y. G. Jeong, *Composites: Part A*, 2011, **42**, 560–566.

(76) H. M. Jeong, M. Y. Choi, Y. T. Ahn, *Macromol. Res.*, 2006, **14**, 312–317.

(77) A. B. Morgan, J. W. Gilman, *J. Appl. Polym. Sci.*, 2003, **87**, 1329–1338.